Eur. J. Mineral., 32, 101–119, 2020
https://doi.org/10.5194/ejm-32-101-2020

European Journal of Mineralogy
Open Access

Unusual silicate mineralization in fumarolic sublimates of the Tolbachik volcano, Kamchatka, Russia – Part 1: Neso-, cyclo-, ino- and phyllosilicates

Nadezhda V. Shchipalkina[1], Igor V. Pekov[1], Natalia N. Koshlyakova[1], Sergey N. Britvin[2,3], Natalia V. Zubkova[1], Dmitry A. Varlamov[4], and Eugeny G. Sidorov[5]

[1]Faculty of Geology, Moscow State University, Vorobievy Gory, 119991 Moscow, Russia
[2]Department of Crystallography, St Petersburg State University, University Embankment 7/9, 199034 St. Petersburg, Russia
[3]Kola Science Center of Russian Academy of Sciences, Fersman Str. 14, 184200 Apatity, Russia
[4]Institute of Experimental Mineralogy, Russian Academy of Sciences, Academica Osypyana ul., 4, 142432 Chernogolovka, Russia
[5]Institute of Volcanology and Seismology, Far Eastern Branch of Russian Academy of Sciences, Piip Boulevard 9, 683006 Petropavlovsk-Kamchatsky, Russia

Correspondence: Nadezhda V. Shchipalkina (estel58@yandex.ru)

Received: 19 June 2019 – Accepted: 1 November 2019 – Published: 29 January 2020

Abstract. This is the initial paper in a pair of articles devoted to silicate minerals from fumaroles of the Tolbachik volcano (Kamchatka, Russia). These papers contain the first systematic data on silicate mineralization of fumarolic genesis. In this article nesosilicates (forsterite, andradite and titanite), cyclosilicate (a Cu,Zn-rich analogue of roedderite), inosilicates (enstatite, clinoenstatite, diopside, aegirine, aegirine-augite, esseneite, "Cu,Mg-pyroxene", wollastonite, potassic-fluoro-magnesio-arfvedsonite, potassic-fluoro-richterite and litidionite) and phyllosilicates (fluorophlogopite, yanzhuminite, "fluoreastonite" and the Sn analogue of dalyite) are characterized with a focus on chemistry, crystal-chemical features and occurrence. Unusual As^{5+}-rich varieties of forsterite, andradite, titanite, pyroxenes, amphiboles and mica are described. General data on silicate-bearing active fumaroles and the diversity and distribution of silicates in fumarole deposits are reported. Evidence for the fumarolic origin of silicate mineralization is discussed.

1 Introduction

Active volcanic fumaroles can be considered natural laboratories which make it possible to study in situ the processes of mineral formation, geochemical behaviour and migration of many chemical elements.

The main minerals in the majority of fumaroles related to active volcanoes are sulfates, halides, oxides and sulfides. Such mineralization was reported in many papers, including review publications. For example, data on the mineralogy of fumaroles were given for Central American volcanoes by Stoiber and Rose (1974), for Kamchatka volcanoes by Serafimova (1979) and for European volcanoes by Balić-Žunić et al. (2016). Relevant literature about fumarolic mineral assemblages from separate active volcanoes includes, e.g. papers by Naughton et al. (1976) – for Kilauea (Hawaii, USA), by Keith et al. (1981) – for Mount St. Helens (Washington, USA), by Africano and Bernard (2000) – for Mount Usu (Japan), by Honnorez et al. (1973) and Campostrini et al. (2011) – for Vulcano (Aeolian Islands, Italy), by Chaplygin et al. (2007) – for Kudryavyi (Iturup, Kuril Archipelago, Russia), and by Serafimova (1992) and Vergasova and Filatov (2016) – for Tolbachik (Kamchatka, Russia).

Despite abundant data on minerals from volcanic fumaroles, silicate mineralization formed in these systems was characterized very scarcely. In particular, this might be due mainly to the proper identification of the origin of silicates from fumarolic deposits (including old, extinct fumaroles).

Even if silicates are in fumarolic vents, they are typically early minerals, which form crusts underlying "classic" sublimate incrustations that include sulfates, halides, oxides, etc. This fact hampers the reliable determination of genesis of silicates and requires an answer to the following question: are they formed with a participation of fumarolic gas or not? Another reason for the difficult identification of the origin of silicates in such mineral-forming systems is the absence of chemical criteria in literature data. Indicative impurities could be geochemical markers showing that a silicate mineral was deposited from the gas phase or, at least, crystallized in the system involving fumarolic gas.

The presence of silicates has been mentioned in fumaroles of several volcanoes. Albite, diopside, sanidine, andalusite, microcline, cordierite and anorthite were reported from a fumarole at Mount St. Augustine (Alaska, USA) (Getahun et al., 1996), tremolite and aegirine ("acmite") in fumaroles at Merapi (Indonesia) (Symonds et al., 1987), aegirine and andradite in fumaroles at Kudryavyi (Tessalina et al., 2008), orthoclase and albite in fumaroles borne by the Northern Breakthrough of the Great Tolbachik Fissure Eruption 1975–1976 (NB GTFE) at Tolbachik (Vergasova and Filatov, 2016), and esseneite and melilite in exhalations within a lava tube from the 2012–2013 eruption of Tolbachik (Sharygin et al., 2018). However, these articles, except for the last cited paper, do not contain data on chemical composition, morphological features and occurrence of silicates in fumarole systems.

It came as a surprise to find a rich and diverse (31 mineral species) silicate mineralization in sublimates of fumaroles related to the Tolbachik volcano. The majority of these minerals was unusual, remarkable in both chemical and crystal-chemical aspects. In the present paper and the companion article we describe these silicates and thus report the first systematic characteristics of silicate mineralization formed in fumaroles at the active volcano. We believe that diversity and chemical originality of silicates are caused by strongly oxidizing conditions of mineral formation and distinct "ore" geochemical specialization of the Tolbachik fumaroles (Pekov et al., 2018a). In the present paper we report data on neso-, cyclo-, ino- and phyllosilicates; the next paper will be devoted to the great variety of tecto-aluminosilicates. The discussion and conclusions concerning fumarolic silicate mineralization in general are given in the companion paper (Shchipalkina et al., 2020).

2 Location

The Tolbachik volcano belongs to the active Klyuchevskaya volcanic group, the greatest from the Kurilo–Kamchatsky volcanic belt. It is located at the central part of the Kamchatka peninsula. In addition to Tolbachik, this group includes two active volcanoes, Klyuchevskoy and Bezymiannyi, and several extinct volcanoes. All of them appeared during the Quaternary a few hundred thousand years ago. The Tolbachik volcanic massif consists of the extinct andesitic volcano Ostryi Tolbachik and active basaltic volcano Ploskiy Tolbachik (Fedotov and Markhinin, 1983).

The widest diversity of silicates was found in the Arsenatnaya fumarole situated at the summit of the second scoria cone of the Northern Breakthrough of the Great Tolbachik Fissure Eruption 1975–1976 (NB GTFE). This cone is a monogenetic volcano about 300 m high and approximately 0.1 km^3 in volume located 18 km SSW of Ploskiy Tolbachik. Its formation started on 9 August 1975 and was completed on 15 September 1975 (Fedotov and Markhinin, 1983). Arsenatnaya is an active fumarole discovered by the authors in July 2012. This fumarole is a linear system (about 15 m long and up to 4 m wide) of mineralized vents located in the interval from 0.3 to 4 m depth under the ground. The temperature inside the vents measured by the authors using a chromel–Alumel thermocouple in 2012–2018 varies from 360 to 490 °C and, in general, increases with depth. Arsenatnaya is the brightest example in the world of the strongly mineralized oxidizing-type fumarole. It was characterized in detail by Pekov et al. (2014, 2018a). Some silicates were also found in other fumaroles located at the second scoria cone of the NB GTFE, including the famous Yadovitaya fumarole described by Vergasova and Filatov (2016).

Rich silicate mineralization also occurs in deposits of extinct fumaroles at Mountain 1004, a scoria cone located 2 km south of the second scoria cone of the NB GTFE. Mountain 1004 is a monogenetic volcano formed as a result of an ancient eruption of Tolbachik, about 2000 years ago (Naboko and Glavatskikh, 1992).

2.1 Host rocks

The main type of rocks forming the second scoria cone of the NB GTFE is a scoria of magnesian basalt with moderate alkalinity. Phenocrysts in this rock include Mg-rich clinopyroxene (diopside and diopside augite with ferruginosity $f = 12$–$20\,\%$), olivine (Fo_{85} – Fo_{90}, $Fo = Mg_2SiO_4$) and, rarely, plagioclase (An_74–An_55, $An = CaAl_2Si_2O_8$) (Fig. S1 in Supplement). The percentage of phenocrysts in this basalt varies from 5 % to 6 %. The groundmass is vitreous with microlites of plagioclase (An_{72}–An_{55}), olivine (Fo_{62}–Fo_{72}), clinopyroxene (with ferruginosity $f = 38\,\%$–$41\,\%$) and spinel-group oxides (Cr-bearing varieties of hercynite and magnetite) (Fedotov and Markhinin, 1983). However, the last days of eruption of the second scoria cone were characterized by effusion of lava with an intermediate petrochemical type, between magnesian basalts and subalkaline alumina-rich basalts. This intermediate-type basalt represents about 10 vol % of the NB GTFE rocks (Fedotov and Markhinin, 1983).

The mineralized pockets of the Arsenatnaya fumarole are located in an area mainly composed by blocks of scoria and volcanic bombs consisting of intermediate-type basalt.

This rock corresponds to subalkaline basalts with the following composition (wt %): K_2O 4.2, Na_2O 1.3, SiO_2 49.8, Al_2O_3 14.2, FeO 13.7, CaO 9.3, MgO 5.1, TiO_2 1.5 and P_2O_5 0.4 (Fedotov and Markhinin, 1983). For comparison, the average chemical composition of the most typical magnesian basalt of the NB GTFE (wt %) is $K_2O + Na_2O$ 3.5, SiO_2 49.5, Al_2O_3 13.4, CaO 11.6, MgO 10.2, FeO 6.7, Fe_2O_3 3.1, MnO 0.2, TiO_2 1.0 and P_2O_5 0.2 (Fedotov and Markhinin, 1983). Our chemical data for the rock hosting the Arsenatnaya fumarole are in accord with data for basalt common for the last period of the second scoria cone activity (Fedotov and Markhinin, 1983). Chemical data for rock-forming minerals and glass from basalt hosting the Arsenatnaya fumarole are given in Table S1 and Fig. S1 (Supplement).

3 Silicate mineralization in Tolbachik fumaroles: general data

The Arsenatnaya fumarole is the major subject of the present study. It is remarkable in mineral diversity. The number of mineral species of exhalation origin and products of their supergene alteration identified is about 210, including 40 insufficiently studied mineral phases (Pekov et al., 2019). Among the sublimate minerals found in the Arsenatnaya fumarole, 26 valid species and five insufficiently studied mineral phases belong to silicates. They include representatives of the majority of subclasses known for natural silicates, in terms of topology of crystal structure, (invalid species names used for simplicity are given in quotation marks at their first usage in the paper): nesosilicates (forsterite, andradite and titanite), cyclosilicates (a Cu,Zn-rich analogue of roedderite), different inosilicates (enstatite, clinoenstatite, diopside, aegirine, aegirine-augite, esseneite, "Cu,Mg-pyroxene", wollastonite, potassic-fluoromagnesio-arfvedsonite, potassic-fluoro-richterite and litidionite), phyllosilicates (fluorophlogopite, yangzhumingite, "fluoreastonite" and the Sn analogue of dalyite) and tectoaluminosilicates (sanidine, anorthoclase, ferrisanidine, anorthite, barium feldspar of the celsian–anorthoclase series, leucite, nepheline, kalsilite, sodalite and hauyne).

Evidence that these minerals do have a fumarolic origin is a key point. The assignment of these silicates to products of deposition from hot fumarole gas or interactions between gas and rocks which compose walls of fumarolic vents is based mainly on two signs. (1) These silicates occur typically as well-shaped crystals in the open space of vents and, which seems especially important, commonly overgrow undoubtedly sublimate minerals (sulfates, arsenates, oxides, halides, etc., including the minerals containing species-defining chalcophile metals) or form intergrowths, usually open-work aggregates, in which silicates and non-silicate minerals demonstrate signs of simultaneous crystallization. (2) The majority of silicate minerals in the Arsenatnaya fumarole, belonging to the most common structure types/archetypes (olivine, garnet, pyroxene, amphibole, mica, feldspar and feldspathoids), are characterized by chemical features unusual for the same minerals from other geological formations. The brightest feature is an enrichment of these silicates (with species-defining Si, Al, Mg, Fe^{3+}, Ca, Na and/or K) by chalcophile and some other ore chemical elements, namely As (the major admixture), Cu, Zn, Sn, Mo and/or W. These ore elements can be in significant amounts (up to several percent by weight) in silicates from the Arsenatnaya fumarole (Table 1) and are species-defining constituents in sublimate minerals belonging to other chemical classes (arsenates, sulfates, oxides, molybdates, borates, etc.) which occur in close intergrowths with the silicates.

The general data on the studied silicates from the Arsenatnaya fumarole are given in Table 1. Silicate mineralization is mainly concentrated in intermediate and deep zones of Arsenatnaya (Fig. 1). The main mineral associations corresponding to different zones are reported in Table 2.

In addition to the above-mentioned aggregates occurring in the open space of vents, some fumarolic silicates (commonly feldspars and fluorophlogopite, occasionally forsterite, kalsilite, sodalite, and hauyne) in the Arsenatnaya fumarole replace basalt. Such replacement rims are observed in near-surface parts of blocks of basalt scoria and volcanic bombs altered by fumarolic gas. The silicates forming these rims demonstrate the same chemical features as their crystals from the deposits originating in the open space of fumarolic vents.

In the Yadovitaya fumarole located at the same second scoria cone of the NB GTFE, only one silicate is known, namely potassic feldspar (sanidine).

At Mountain 1004 there are three paleofumarolic fields: the southern, southwestern and western fields, all bearing rich Cu and sporadic Pb mineralization including sublimate tenorite and anglesite and secondary, supergene atacamite, antlerite, chrysocolla, volborthite, mottramite, pyromorphite, etc. (Serafimova et al., 1994; Pekov et al., 2018b). We believe that the amount and diversity of oxy-salts and chlorides of chalcophile elements was greater here; however, many minerals disappeared with time because of their instability under atmospheric conditions. Nevertheless, the silicate mineralization that is stable under weathering is quite rich there. For these ancient fumarolic fields, diopside, enstatite, albite, orthoclase, leucite, hauyne, pargasite, phlogopite and sericite were mentioned and considered to belong to the post-eruptive association formed at temperatures below 600–800 °C (Naboko and Glavatskykh, 1992). Our studies of paleofumarolic incrustations from Mountain 1004 show the presence of the following silicates: diopside, enstatite, fluorophlogopite, indialite, sanidine, anorthoclase, leucite, and hauyne. The wide distribution of the primary and secondary copper oxy-salts tenorite and atacamite closely associated with these minerals and the presence of admixed Cu in these silicates (see below) may indirectly confirm that these silicate

Table 1. Silicate minerals from Tolbachik fumaroles.

Mineral	Simplified formula	Structure type or archetype	Crystal system	Unit-cell parameters*	As_2O_5 content (up to, wt. %)	Some other typical impurities (up to, wt. %)
Forsterite	$Mg_2[SiO_4]$	Olivine	Orthorhombic	$a = 4.762(1) - 4.772(4)$, $b = 5.967(5) - 5.983(1)$, $c = 10.231(2) - 10.262(10)$ Å, $V = 291.5(1) - 292.2(5)$ Å^3	16.0	CuO – 0.4 P_2O_5 – 12.8
Andradite	$Ca_3Fe^{3+}_2[SiO_4]_3$	Garnet	Cubic	$a = 12.068(5)$ Å, $V = 1757.5(3)$ Å^3	3.3	SnO_2 – 6.0
Titanite	$CaTiO[SiO_4]$	Titanite	Monoclinic	–	6.4	SnO_2 – 3.7
Indialite[1]	$Mg_2Al_3(AlSi_5O_{18})$	Beryl	Hexagonal	$a = 9.795(5)$, $c = 9.362(7)$, $V = 777.8(9)$ Å^3	not detected	
"Cu,Zn-rich analogue of roedderite"[2]	$(Na, K, \square)_3(Mg, Zn, Cu)_{5-x}[Si_{12}O_{30}]$	Osumilite	Hexagonal	–	not detected	CuO – 6.9 ZnO – 8.1
Enstatite	$Mg_2[Si_2O_6]$	Orthopyroxene	Orthorhombic	$a = 5.181(7)$, $b = 8.817(11)$, $c = 18.23(2)$ Å, $V = 832.7(1)$ Å^3	not detected	CuO – 0.5
Clinoenstatite	$Mg_2[Si_2O_6]$	Clinopyroxene	Monoclinic	$a = 9.66(6)$, $b = 8.89(4)$, $c = 5.22(3)$ Å, $\beta = 108.6(8)^\circ$, $V = 426.3(2)$ Å^3	2.5	CuO – 0.5
Diopside	$CaMg[Si_2O_6]$	Clinopyroxene	Monoclinic	$a = 9.7468(15)$, $b = 8.8797(14)$, $c = 5.2819(8)$ Å, $\beta = 105.906(2)^\circ$, $V = 439.64(12)$ Å^3	2.6	CuO – 1.2 ZnO – 0.3 SnO_2 – 7.0
Aegirine	$NaFe^{3+}[Si_2O_6]$	Clinopyroxene	Monoclinic	$a = 9.702(2)$, $b = 8.831(2)$, $c = 5.304(1)$ Å, $\beta = 107.37(2)^\circ$, $V = 433.7(1)$ Å^3	0.8	SnO_2 – 0.3
Aegirine-augite	$(Na, Ca)(Fe^{3+}, Mg)[Si_2O_6]$	Clinopyroxene	Monoclinic	–	1.0	
Esseneite	$CaFe^{3+}[AlSiO_6]$	Clinopyroxene	Monoclinic	–	2.1	

Table 1. Continued.

Mineral	Simplified formula	Structure type or archetype	Crystal system	Unit-cell parameters*	As_2O_5 content (up to, wt. %)	Some other typical impurities (up to, wt. %)
Cu,Mg-pyroxene	$CuMg[Si_2O_6]$	Orthopyroxene	Orthorhombic	$a = 5.24(4)$, $b = 8.87(1)$, $c = 18.25(3)$ Å, $V = 848.2(1)$ Å^3	not detected	ZnO – 3.2
Wollastonite	$Ca_3[Si_3O_9]$	Wollastonite	Triclinic	–	0.4	
Potassic-fluoro-magnesio-arfvedsonite	$KNa_2(Mg_4Fe^{3+})[Si_8O_{22}]F_2$	Amphibole	Monoclinic	–	2.4	CuO – 1.7 ZnO – 0.8 SnO_2 – 1.2
Potassic-fluoro-richterite	$KNaCaMg_5[Si_8O_{22}]F_2$	Amphibole	Monoclinic	$a = 9.873(2)$, $b = 18.069(3)$, $c = 5.252(2)$ Å, $\beta = 104.63(3)°$, $V = 906.3(3)$ Å^3	3.6	SnO_2 – 0.5
Litidionite	$KNaCu[Si_4O_{10}]$	Fenaksite	Triclinic	$a = 7.00(3)$, $b = 8.01(3)$, $c = 9.81(3)$ Å, $\alpha = 105.5(2)$, $\beta = 100.1(3)$, $\gamma = 113.7(4)°$, $V = 459(3)$ Å^3	not detected	ZnO – 0.3
Fluorophlogopite	$KMg_3[AlSi_3O_{10}]F_2$	Mica	Monoclinic	$a = 5.3095(7)$, $b = 9.2082(13)$, $c = 10.1358(12)$ Å, $\beta = 100.101(15)°$, $V = 485.5(4)$ Å^3	5.1	CuO – 1.0 ZnO – 1.7 SnO_2 – 0.8 P_2O_5 – 0.9
Yangzhumingite	$KMg_{2.5}[Si_4O_{10}]F_2$	Mica	Monoclinic	$a = 5.351(21)$, $b = 9.244(24)$, $c = 10.20(3)$ Å, $\beta = 100.4(3)°$, $V = 496.2(4)$ Å^3	0.6	CuO – 1.4
"Fluoreastonite"	$KMg_2Al[Al_2Si_2O_{10}]F_2$	Mica	Monoclinic	–	not detected	
"Sn analogue of dalyite"[2]	$K_2Sn[Si_6O_{15}]$	Dalyite	Triclinic	–	not detected	
Sanidine	$K[AlSi_3O_8]$	Feldspar	Monoclinic	$a = 7.1985(4) - 7.2181(5)$, $b = 13.0575(5) - 13.1111(3)$, $c = 7.1975 - 7.2134$, $\beta = 113.77(4) - 113.94(2)°$, $V = 726.9(1) - 735.6(3)$ Å^3	36.0	CuO – 0.6 ZnO – 0.4

Table 1. Continued.

Mineral	Simplified formula	Structure type or archetype	Crystal system	Unit-cell parameters *	As_2O_5 content (up to, wt. %)	Some other typical impurities (up to, wt. %)
Ferrisanidine	$K[Fe^{3+}Si_3O_8]$	Feldspar	Monoclinic	$a = 8.679(5)$, $b = 13.141(10)$, $c = 7.326(6)$ Å, $\beta = 116.2(1)°$, $V = 749.3(1)$ Å^3	not detected	
Anorthoclase	$(Na, K)[AlSi_3O_8]$	Feldspar	Triclinic	$a = 8.20(3)$, $b = 12.87(3)$, $c = 7.10(2)$ Å, $\alpha = 91.7(1)$, $\beta = 116.1(2)$, $\gamma = 90.2(2)°$, $V = 673.2(5)$ Å^3	6.3	
Albite	$Na[AlSi_3O_8]$	Feldspar	Triclinic	$a = 8.189(7)$, $b = 12.896(13)$, $c = 7.120(5)$ Å, $\alpha = 92.8(1)$, $\beta = 116.1(2)$, $\gamma = 90.3(2)°$, $V = 674.6(1)$ Å^3	–	
Anorthite	$Ca[Al_2Si_2O_8]$	Feldspar	Triclinic	–	1.4	
"Barium feldspar"	$Ba[Al_2Si_2O_8]$	Feldspar	Monoclinic	–	not detected	
Nepheline	$KNa_3[AlSiO_4]_4$	Kalsilite	Hexagonal	–	not detected	
Kalsilite	$K[AlSiO_4]$	Kalsilite	Hexagonal	$a = 5.1562(5)$, $c = 8.6888(11)$ Å, $V = 200.0(6)$ Å^3	6.6	ZnO – 1.0
Leucite	$K[AlSi_2O_6]$	Leucite	Tetragonal?	–	10.4	CuO – 0.3 P_2O_5 – 0.9
Sodalite	$Na_8[Al_6Si_6O_{24}]Cl_2$	Sodalite	Cubic	$a = 8.870(3)$ Å, V =700.3(2) Å^3	1.8	CuO – 0.4
Hauyne	$Na_6Ca_2[Al_6Si_6O_{24}](SO_4)_2$	Sodalite	Cubic	$a = 9.113(2)$ Å, $V = 756.6(3)$ Å^3	2.5	CuO – 0.8 MoO_3 –4.2 WO_3 – 1.7

Note. Dash means the absence of unit-cell data (for minerals forming tiny individuals or thin zones in zoned crystals of other silicates). Names of invalid or insufficiently studied minerals are given in quotation marks. [1] Indialite was found only at Mountain 1004. [2] Minerals identified using Raman spectroscopy, without X-ray diffraction data.

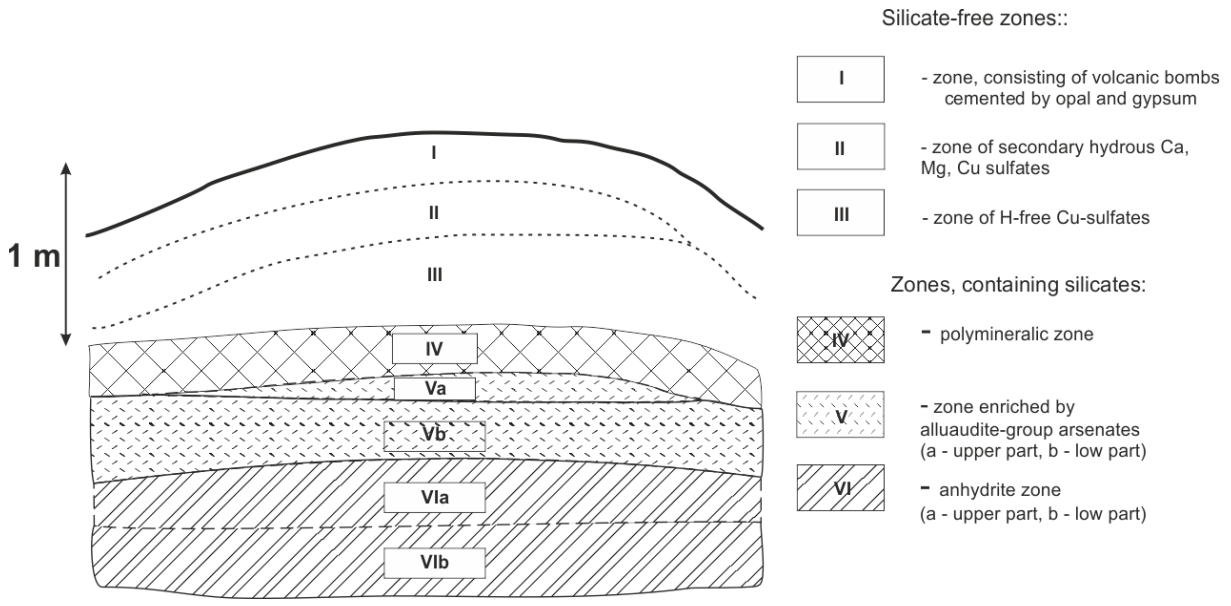

Figure 1. Schematic section across the northern part of the Arsenatnaya fumarole. The scheme is drawn after Pekov et al. (2018a). The detailed description of each zone is given in the cited paper. The mineral diversity of zones containing silicates is listed in Table 3.

crusts could form with participation of fumarolic gas. However, with the formation mechanism of these minerals not being well identified, we only assign it to the post-eruptive stages. Therefore, we prefer to discuss this mineralization separately from silicates from the Arsenatnaya fumarole, for which the crystallization in the oxidizing-type system with ore geochemical specialization seems doubtless.

4 Experimental procedures

The minerals described here were studied by scanning electron microscopy (SEM), electron-microprobe analysis (EMPA, WDS and EDS modes), powder and single-crystal X-ray diffraction, and Raman spectroscopy.

The SEM studies and quantitative EMPA were conducted using a digital scanning electron microscope CamScan MV2300 (VEGA TS 5130MM) with an EDS INCA Energy 350 analytical system at the Laboratory of Analytical Methods, Institute of Experimental Mineralogy of the Russian Academy of Sciences, Chernogolovka, and a JEOL JXA-8230 microprobe instrument (EDS and WDS modes) at the Laboratory of Analytical Techniques of High Spatial Resolution, Dept. of Petrology, Moscow State University, Moscow, Russia. Standard operating conditions included an accelerating voltage of 20 kV and beam current of 0.7 nA (EDS mode) or 20 nA (WDS mode) in both cases. The standards used for quantitative analysis are potassic feldspar for K (K line), albite for Na (K line), anorthite and wollastonite for Ca (K line), $BaSO_4$ and BaF_2 for Ba (L line), $SrSO_4$ for Sr (L line), diopside and MgF_2 for Mg (K line), Mn for Mn (K line), Cu for Cu (K line), ZnS and Zn for Zn (K line), anorthite and Al_2O_3 for Al (K line), Fe for Fe (K line), Cr_2O_3 and Cr for Cr (K line), V for V (K line), $KTiOPO_4$ and Ti for Ti (K line), anorthite and SiO_2 for Si (K line), SnO_2 and Sn for Sn (K line), GaAs and InAs for As (K line), $KTiOPO_4$ and $LaPO_4$ for P (K line), ZnS and FeS_2 for S (K line), $CaMoO_4$ for Mo (L line), $CaWO_4$ for W (L line), CaF_2 and MgF_2 for F (K line), and NaCl for Cl (K line). Results are given in Tables 3 and S2.

A full sphere of three-dimensional X-ray diffraction (XRD) data for studied single-crystal samples were collected using Mo$K\alpha$ radiation ($\lambda = 0.71073$ Å) at room temperature on an Xcalibur S CCD diffractometer. Data reduction was performed using CrysAlisPro version 1.171.37.35 (Agilent Technologies, 2014).

Powder X-ray diffraction data were collected using a Rigaku R-AXIS Rapid II diffractometer (image plate), Co$K\alpha_1/\alpha_2$ ($\lambda = 1.79021$ Å) radiation, 40 kV, 15 mA, a rotating anode with microfocus optics, Debye–Scherrer geometry, $d = 127.4$ mm and exposure 15 min. The data were integrated using the software package Osc2Tab (Britvin et al., 2017). Intensities of diffraction reflections and unit-cell parameters for minerals were calculated by means of the STOE WinXPOW v.2.08 program suite. The JANA program package (Petříček et al., 2014) was used for the refinement of crystal structures by the Rietveld method.

The Raman spectra were recorded using an EnSpectr R532 spectrometer with a green laser (532 nm) at room temperature. The power of the laser beam on the sample was about 7 mW. The spectrum was processed using the EnSpectr expert mode program in the range from 100 to 4000 cm^{-1} with the use of a holographic diffraction grat-

Table 2. Silicates (the most widespread species are marked in bold) and main associated minerals in different mineralized zones in the Arsenatnaya fumarole.

No.	Zone	Silicates	Main associated minerals
IV	Polymineralic zone	**As-bearing sanidine**, hauyne, sodalite, fluorophlogopite, kalsilite, aegirine, potassic-fluoro-magnesio-arfvedsonite, potassic-fluoro-richterite, yanzhumingite, diopside, litidionite, clinoenstatite, "pyroxene", fluoreastonite, titanite, Cu,Zn-rich analogue of roedderite, Sn analogue of dalyite, ferrisanidine	aphthitalite, metathenardite, cassiterite, various copper arsenates, johillerite, svabite, hematite, tilasite, filatovite, sylvite, halite, tenorite, pseudobrookite, corundum, gahnite, anhydrite, tridymite
Va and Vb	Zone enriched in alluaudite-group arsenates	**sanidine**, **fluorophlogopite**, hauyne, sodalite, leucite, diopside, nepheline, "fluoroeastonite", aegirine-augite	calciojohillerite, badalovite, nickenichite, johillerite, hematite, tilasite, svabite, cassiterite, pseudobrookite, alarsite, durangite, sylvite, tridymite
VIa	Anhydrite zone (upper part)	**fluorophlogopite**, diopside, anorthoclase, esseneite, forsterite, hauyne, anorthite	anhydrite, hematite, cassiterite, fluorapatite, arsenowagnerite, tilasite, magnesioferrite, tridymite
VIb	Anhydrite zone (lower part)	**diopside**, forsterite, andradite, enstatite, esseneite, hauyne, (including Mo,W-bearing variety), anorthoclase, titanite, wollastonite, barium feldspar	anhydrite, hematite, members of svabite–fluorapatite and berzeliite–schäferite series, calciojohillerite, magnesioferrite, ludwigite

The arrangement of described zones is shown in Fig. 2. Names of invalid minerals are given in quotation marks.

ing with 1800 lines cm^{-1} and a resolution equal to 5–8 cm^{-1}. The diameter of the focal spot on the sample was about 10 µm. Raman spectra were acquired on polycrystalline samples.

5 Characterization of minerals: neso-, cyclo-, ino- and phyllosilicates

5.1 Nesosilicates

The overwhelming number of nesosilicates in the Arsenatnaya fumarole occur in Zone VIb (Table 2), excluding minor finds of titanite in Zone IV.

5.1.1 Forsterite

Forsterite is a typical mineral of the deepest zones of the Arsenatnaya fumarole. It associates with hematite, hauyne, anhydrite and members of the svabite–fluorapatite series. The morphology of its colourless or pale pinkish transparent crystals (up to 0.1 mm in size) is diverse. There are perfect prismatic crystals with well-developed faces of two prisms (Fig. 2a), lens-shaped crystals (Fig. 2b), twins and trillings (110) (Fig. 2c). The bright red forsterite crystals (< 50 µm in size) typically form open-work aggregates with hematite. Such vivid colour is due to the inclusions of fine-powder hematite (Fig. 3). In Zone IVb the major silicate mineral associated with forsterite is hauyne. Both form white crusts replacing basalt scoria and open-work clusters in cavities. Lamellar aggregations of forsterite "cemented" by hauyne (Fig. 2d) were also observed.

The most typical forsterite from Arsenatnaya is chemically close to end-member Mg_2SiO_4. Some samples of "ordinary" forsterite from this locality contain the following impurities (up to, wt %): MnO 2.4, Fe_2O_3 2.3, As_2O_5 2.4, P_2O_5 2.4 and CuO 0.4 (see also analysis 1, Table 3) (iron is considered trivalent due to strongly oxidizing conditions of mineral formation in the Tolbachik fumaroles; Pekov et al., 2018a).

One of the studied samples of forsterite is outstanding in both chemical and crystal chemical aspects. There are zoned crystals containing up to 16.0 wt % As_2O_5 and up to 12.9 wt % P_2O_5. The empirical formulae (calculated on the basis of four O atoms per formula unit, apfu) corresponding to composition of the P- and As-richest zones are $(Mg_{1.82}Mn_{0.01})_{\Sigma 1.83}[(Si_{0.58}P_{0.26}As_{0.14})_{\Sigma 0.98}O_4]$ and $(Mg_{1.88}Mn_{0.01})_{\Sigma 1.89}[(Si_{0.69}As_{0.20}P_{0.09})_{\Sigma 0.98}O_4]$ respectively (Table 3, analyses 2 and 3). A special paper is devoted to the crystal chemistry and genetic features of this variety of forsterite – the P- and As-richest natural olivine (Shchipalkina et al., 2019).

5.1.2 Andradite

Minerals of the garnet supergroup are mainly represented in Arsenatnaya by members of the berzeliite $(Ca_2Na)Mg_2(AsO_4)_3$–schäferite $(Ca_2Na)Mg_2(VO_4)_3$ solid–solution series, widespread in the Zones VIa and VIb of the fumarole (Pekov et al., 2018). The silicate garnet andradite is found in the same association (Table 2) but is not so abundant. Andradite forms crystal clusters or crusts overgrowing hematite and usually covered by anhydrite (Fig. 4a, b). The zonation of its brown or dark brownish-red crystals is due to variations in Fe : Al ratio and admixed Sn content (Fig. 4b). The content of grossu-

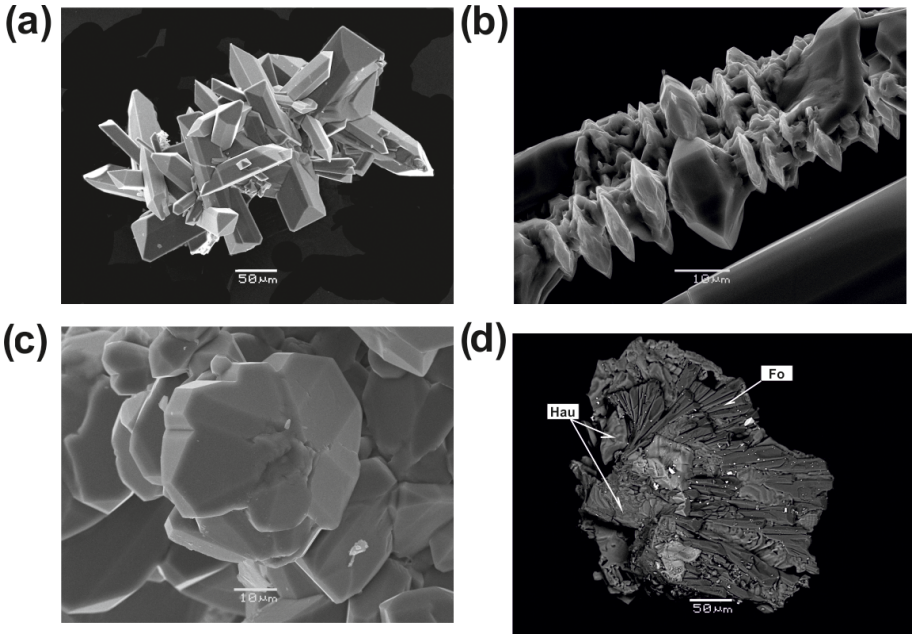

Figure 2. Morphology of forsterite from the Arsenatnaya fumarole: **(a)** aggregate of well-shaped prismatic crystals, **(b)** lens-shaped crystals overgrowing acicular crystals of anhydrite, **(c)** trilling on (110), **(d)** fragment of aggregate of forsterite "cemented" by hauyne. Secondary electron (SE) images.

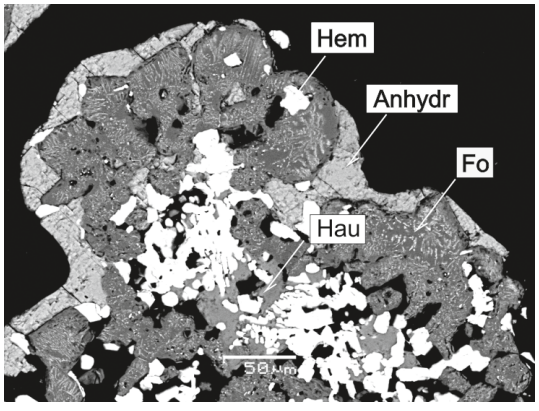

Figure 3. Red forsterite (saturated with hematite inclusions) intimately associated with hauyne (Hau) and hematite (Hem) and covered by a crust of anhydrite (Anhydr). Arsenatnaya fumarole. Backscattered electron (BSE) image.

lar component in andradite from Arsenatnaya reaches 34 mol %. The mineral contains up to 3.3 wt % As_2O_5 and up to 6.0 wt % SnO_2 (Table 3, analyses 4 and 5). Andradite and diopside are significant concentrators of Sn in Zone VIb. Typical empirical formulae of the Al-poor and Al-rich varieties of andradite from Arsenatnaya are $(Ca_{2.89}Mg_{0.11})_{\sum 3.00}(Fe^{3+}_{1.81}Sn_{0.08}Mg_{0.05}Al_{0.02})_{\sum 1.96}[(Si_{2.84}As^{5+}_{0.15})_{\sum 2.99}O_{12}]$ and $(Ca_{2.91}Mg_{0.08})_{\sum 2.99}(Fe^{3+}_{1.63}Sn_{0.07}Ti_{0.03}Al_{0.27})_{\sum 2.00}[(Si_{2.88}Al_{0.12})_{\sum 3.00}O_{12}]$ respectively.

5.1.3 Titanite

Titanite is rare in the Arsenatnaya fumarole. It occurs as tiny crystals, grains or crystal clusters up to 70 µm across in arsenate silicate crusts replacing basalt scoria (Fig. 5). The most typical associated minerals are sanidine, sodalite and svabite. The representative empirical formulae of two chemical varieties of titanite from Arsenatnaya are $Ca_{0.97}(Ti_{0.78}Al_{0.10}Fe^{3+}_{0.07}Mg_{0.03}Sn_{0.03})_{\sum 1.01}[(Si_{0.97}As^{5+}_{0.04})_{\sum 1.01}O_4](O_{0.85}F_{0.15})$ and $Ca_{0.98}(Ti_{0.86}Fe^{3+}_{0.07}Al_{0.05}Sn_{0.03}V_{0.02})_{\sum 1.03}[Si_{0.97}As^{5+}_{0.03}O_4]O_{0.99}$ (Table 3, analyses 6 and 7).

5.1.4 Cyclosilicate, the Cu,Zn-rich analogue of roedderite

A member of the osumilite group with the simplified formula $(Na, K, \square)_3(Mg, Zn, Cu)_{5-x}[Si_{12}O_{30}]$ (Table 1) was found in Zone IV of Arsenatnaya. It forms hexagonal prismatic crystals combined in parallel intergrowths up to 50 µm in size in association with tridymite, litidionite, cassiterite and As-bearing sanidine (Fig. 6). The assignment of this mineral to the osumilite structure type on the basis of chemical composition and crystal morphology was confirmed by the Raman spectrum (Fig. 6). Chemical data make it possible to assume that the mineral is a Zn- and Cu-rich variety of roedderite, ideally $KNaMg_5[Si_{12}O_{30}]$ (Alietti et al., 1994), or its hypothetic Mg−(Cu/Zn)-ordered analogue.

Table 3. Typical chemical composition of forsterite (Fo), andradite (Adr), titanite (Ttn), the Cu,Zn-rich analogue of roedderite (CuZn-Rdr), enstatite (En), clinoenstatite (Cln), aegirine (Aeg), diopside (Di), esseneite (Ess), Cu,Mg-pyroxene (Cu-Px), potassic-fluoro-magnesio-arfvedsonite (Arf), potassic-fluoro-richterite (Rch), litidionite (Ltd), fluorophlogopite (FPhlg), yanzhuminite (Ynzh), fluoreastonite (FEst) and the Sn analogue of dalyite (Sn-Dlt) from the Arsenatnaya fumarole. The samples containing significant impurities of ore components are included.

Component	1	2	3	4	5	6	7	8	9	10	11	12	13	14	15	16
	Fo	Fo	Fo	Adr	Adr	Ttn	Ttn	CuZn-Rdr	En	Cln	Aeg	Di	Di	Di	Di	Ess
	(wt %)															
SiO_2	39.49	24.32	28.41	31.74	33.63	29.10	25.99	69.69	58.42	58.03	50.41	51.79	36.47	52.39	47.12	33.52
TiO_2	–	–	–	0.31	–	31.26	28.44	–	–	–	1.53	0.27	–	–	0.20	1.96
SnO_2	–	–	–	5.99	2.35	1.97	3.72	–	–	–	0.32	–	7.03	–	–	0.58
Al_2O_3	0.03	–	–	2.24	0.16	2.60	0.14	–	0.40	0.18	0.85	0.43	10.01	–	1.94	16.21
Cr_2O_3	–	–	–	–	–	0.21	–	–	–	–	–	–	–	–	–	–
Fe_2O_3	0.68	–	–	26.27	28.56	2.91	4.73	–	0.87	0.74	30.66	2.52	12.87	6.39	18.07	17.93
MnO	0.70	0.32	0.34	–	–	–	–	–	0.72	1.64	0.21	–	–	–	0.59	0.42
ZnO	–	–	–		–	–	–	8.12	–	–	–	–	–	0.31	–	–
CuO	0.35	–	–	–	–	–	–	6.85	0.39	0.31	–	–	–	–	0.37	–
MgO	55.46	51.00	52.19	0.44	1.31	0.59	1.42	7.86	38.56	37.06	1.23	18.04	9.41	15.19	8.37	5.82
CaO	–	–		31.15	32.00	27.23	26.83	–	0.84	0.51	1.21	21.81	22.82	20.92	22.07	22.94
Na_2O	–	–	–	–	–	–	–	3.28	–	0.06	12.78	1.85	–	2.41	0.45	0.21
K_2O	–	–	–	–	–	–	–	3.94	–	–	0.31	0.22	–	–	–	–
P_2O_5	0.79	12.87	4.36		–	0.11	–	–	–	–	–	–	–	–	–	–
V_2O_5	–	0.16	0.32	–	–	–	–	–	–	–	–	–	–	–	–	–
As_2O_5	3.26	11.38	16.00	0.43	3.31	2.26	6.41	–	–	2.48	0.78	2.64	–	1.50	–	–
Sb_2O_5	–	–	–	–	–	–	–	–	–	–	–	–	–	–	–	–
F	–	–	–	–	–	1.39	1.50	–	–	–	–	–	–	–	–	–
Cl	–	–	–	–	–	–	–	–	–	–	–	–	–	–	–	–
$O=(F,Cl)_2$				–	–	0.59	0.63									
Total	100.76	100.05	101.62	98.57	101.32	99.04	98.55	99.74	100.20	101.01	100.29	99.57	98.61	99.11	99.18	99.59
	Empirical formulae															
Si	0.93	0.58	0.69	2.78	2.84	0.97	0.90	12.45	1.97	1.96	1.93	1.90	1.47	1.95	1.82	1.31
Ti	–	–	–	0.02	–	0.78	0.74	–	–	–	0.04	0.01	–	–	0.01	0.06
Sn	–	–	–	0.21	0.08	0.03	0.05	–	–	–	0.00	–	0.11	–	–	0.01
Al	0.00	–	–	0.23	0.02	0.10	0.01	–	0.02	0.01	0.04	0.02	0.47	–	0.09	0.75
Cr^{3+}	–	–	–	–	–	0.01	–	–	–	–	–	–	–	–	–	–
Fe^{3+}	0.01	–	–	1.73	1.81	0.07	0.12	–	0.02	0.02	0.89	0.07	0.39	0.18	0.52	0.53
Mn	0.01	0.01	0.01	–	–	–	–	–	0.02	0.05	0.01	–	–	–	0.02	0.01
Zn	–	–	–	–	–	–	–	1.07	–	–	–	–	–	0.01	–	–
Cu	0.01	–	–	–	–	–	–	0.92	0.01	0.01	–	–	–	–	0.01	–
Mg	1.95	1.82	1.88	0.06	0.16	0.03	0.07	2.09	1.94	1.86	0.07	0.99	0.56	0.84	0.48	0.34
Ca	–	–	–	2.92	2.89	0.97	0.99	–	0.03	0.02	0.05	0.86	0.98	0.83	0.91	0.96
Na	–	–	–	–	–	–	–	1.14	–	0.00	0.95	0.13	–	0.17	0.03	0.02
K	–	–	–	–	–	–	–	0.92	–	–	0.02	0.01	–	–	–	–
P^{5+}	0.02	0.26	0.09	–	–	0.00	–	–	–	–	–	–	–	–	–	–
V^{5+}	–	0.00	–	–	–	–	–	–	–	–	–	–	–	–	–	–
As^{5+}	0.04	0.14	0.20	0.02	0.15	0.04	0.12	–	–	0.04	0.02	0.05	–	0.03	–	–
Sb^{5+}	–	–	–	–	–	–	–	–	–	–	–	–	–	–	–	–
F^-	–	–	–	–	–	0.15	0.16	–	–	–	–	–	–	–	–	–
Cl^-	–	–	–	–	–	–	–	–	–	–	–	–	–	–	–	–
$\sum cat$	2.97	2.81	2.87	7.97	7.95	3.00	3.00	18.59	4.01	3.97	4.02	4.04	3.98	4.01	3.89	3.99
BoFC	4 O	4 O	4O	12 O	12 O	[1]	[1]	30 O	6 O	6 O	6 O	6 O	6 O	6 O	6 O	6 O

5.2 Inosilicates

5.2.1 Enstatite and clinoenstatite

These two dimorphs of $Mg_2[Si_2O_6]$ occur in different zones of the Arsenatnaya fumarole. Enstatite originates mainly from Zone VI while clinoenstatite occurs hypsometrically higher, in Zone IV. The belonging of a mineral with formula $Mg_2[Si_2O_6]$ to ortho- or clinopyroxene was determined by single-crystal X-ray diffraction. The unit-cell parameters for both minerals are given in Table 1.

Enstatite forms well-shaped prismatic (Fig. 7a) transparent colourless to pale yellowish crystals associated with fluorophlogopite, hematite and members of the fluorapatite–svabite series. Its crystals also overgrow diopside crystals (Fig. 8a). Chemically, the mineral is typically close to the end-member. In some samples the following impurities were detected (up to, wt %): CaO and MnO 1.0, CuO 0.4, Fe_2O_3 1.9, and Al_2O_3 1.3. Arsenic was not detected in enstatite.

Clinoenstatite occurs as transparent colourless or greenish columnar to acicular crystals up to 0.1 mm long (Fig. 7b).

Table 3. Continued.

Component	17	18	19	20	21	22	23	24	25	26	27	28	29	30
	Cu-Px	Cu-Px	Cu-Px	Wol	Arf	Rch	Ltd	FPhlg	FPhlg	FEst	Ynzh	Ynzh	Sn-Dlt	Sn-Dlt
	(wt %)													
SiO_2	52.47	50.8	50.45	50.59	52.85	54.82	58.77	32.25	37.87	30.73	55.44	54.11	62.40	63.22
TiO_2	–	–	–	–	0.17	0.66	–	0.83	1.46	0.44	0.08	0.39	–	5.22
SnO_2	–	–	–	–	–	0.53	–	–	–	–	–	–	18.68	11.28
Al_2O_3	1.26	0.77	1.17	–	0.06	1.96	–	16.89	15.17	33.77	2.36	1.08	0.08	–
Cr_2O_3	–	–	–	–	–	–	–	–	–	–	–	–	–	–
Fe_2O_3	2.75	1.50	2.25	0.70	5.21	7.57	0.11	1.21	1.79	1.50	0.72	2.07	1.76	1.96
MnO	–	–	–	0.32	0.13	–	–	0.03	–	–	0.10	–	–	–
ZnO	0.58	1.32	2.52	–	0.79	–	0.33	–	–	–	–	0.70	–	–
CuO	17.77	20.93	24.71	–	1.72	–	19.56	0.38	1.04	–	0.47	1.43	–	–
MgO	26.96	24.03	18.10	0.15	18.20	19.90	–	26.34	25.02	19.09	27.14	24.01	–	–
CaO	0.10	–	1.35	46.03	1.90	6.07	–	–	–	–	–	–	–	–
Na_2O	–	–	–	–	7.23	4.50	8.10	–	–	–	0.24	1.25	0.47	0.26
K_2O	–	–	–	–	5.29	3.74	11.31	10.21	10.50	7.69	8.36	9.65	15.71	16.19
P_2O_5	–		–	–	–	–	–	0.52	0.18	–	–	–	–	–
V_2O_5	–	–	–	–	0.28	–	0.28	–	–	–	–	–	–	0.31
As_2O_5	–	–	–	0.37	2.41	–	–	5.10	1.24	–	–	0.64	–	–
Sb_2O_5	–	–	–	–	–	–	–	–	–	–	–	–	–	1.93
F	–	–	–	–	4.07	3.80	–	8.58	7.98	5.39	9.17	8.76	–	–
Cl	–	–	–	–	0.23	–	–	–	–	–	–	–	–	–
$O=(F, Cl)_2$					1.76	1.60		3.61	3.36	2.27	3.86	3.69	–	–
Total	101.89	99.35	100.55	98.16	98.78	101.95	98.46	98.73	98.89	96.34	100.22	100.40	99.10	100.37
	Empirical formulae													
Si	1.91	1.92	1.96	2.99	7.65	7.58	3.97	2.35	2.74	2.23	3.76	3.76	6.15	5.99
Ti	–	–	–	–	0.02	0.07	–	0.05	0.08	0.02	0.00	0.02	–	0.37
Sn	–	–	–	–	–	0.03	–	–	–	–	–	–	0.73	0.43
Al	0.05	0.03	0.05	–	0.01	0.32	–	1.45	1.29	2.89	0.19	0.09	0.01	–
Cr^{3+}	–	–	–	–	–	–	–	–	–	–	–	–	–	–
Fe^{3+}	0.08	0.04	0.07	0.03	0.57	0.79	0.01	0.07	0.10	0.08	0.04	0.11	0.13	0.14
Mn	–	–	–	0.02	0.02	–	–	0.01	–	–	0.01	–	–	–
Zn	0.02	0.04	0.07	–	0.08	–	0.02	–	–	–	–	0.04	–	–
Cu	0.49	0.60	0.72	–	0.19	–	1.00	0.02	0.06	–	0.02	0.08	–	–
Mg	1.47	1.35	1.05	0.01	3.93	4.10	–	2.87	2.69	2.06	2.74	2.49	–	–
Ca	0.00	–	0.06	2.92	0.29	0.90	–	–	–	–	–	–	–	–
Na	–	–	–	–	2.03	1.21	1.06	0.07	–	–	0.03	0.17	0.09	0.05
K	–	–	0.02		0.98	0.66	0.97	0.95	0.97	0.71	0.72	0.86	1.97	1.96
P^{5+}	–	–	–	–	–	–	–	0.03	0.01	–	–	–	–	–
V^{5+}	–	–	–	–	0.03	–	0.01	–	–	–	–	–	–	0.02
As^{5+}	–	–	–	0.01	0.18	–	–	0.19	0.05	–	–	0.02	–	–
Sb^{5+}	–	–	–	–	–	–	–	–	–	–	–	–	–	0.07
F^-	–	–	–	–	1.86	1.66	–	1.98	1.82	1.24	1.97	1.93	–	–
Cl^-	–	–	–	–	0.06	–	–	–	–	–	–	–	–	–
$\sum cat$	4.02	3.98	4.00	5.98	15.98	15.66	7.04	8.06	7.99	7.99	7.51	7.64	9.08	9.03
BoFC	6 O	6 O	6 O	9 O	[2]	[2]	10 O	[3]	[3]	[3]	[3]	[3]	15 O	15 O

Note: Dash means "below detection limit". BoFC means a basis of formula calculation, i.e. number of oxygen atoms per formula unit (apfu), except for [1] for titanite sum of all cations = 3 apfu, [2] for amphiboles $\sum B + C + T = Na + Ca + Si + P + As + V + Al + Fe + Ti + Sn + Zn + Cu + Mn + Mg = 15$ apfu in accordance with the general formula of amphiboles $AB_2C_5[T_8O_{22}]W_2$ (Hawthorne et al., 2012), and [3] for mica O + F = 12. Names of invalid minerals are given in quotation marks.

The main crystal forms are {011}, {010} and {110}. The major associated minerals are svabite, sodalite and sanidine. The main impurities in clinoenstatite from the Arsenatnaya fumarole are (up to, wt %): 1.6 MnO, 0.3 CuO, 0.7 Fe_2O_3 and 0.2 Al_2O_3. The comparison of unit-cell parameters of our mineral and low and high clinoenstatite (Smyth, 1974) shows that our pyroxene is low clinoenstatite.

5.2.2 Clinopyroxenes of the diopside–esseneite–aegirine solid–solution system

Members of the diopside–esseneite–aegirine solid–solution system are widespread in hematite–clinopyroxene–anhydrite incrustations in Zones Vb, VIa and VIb. The main pyroxene of this system is diopside. Typically it forms practically monomineralic, or with anhydrite, incrustations con-

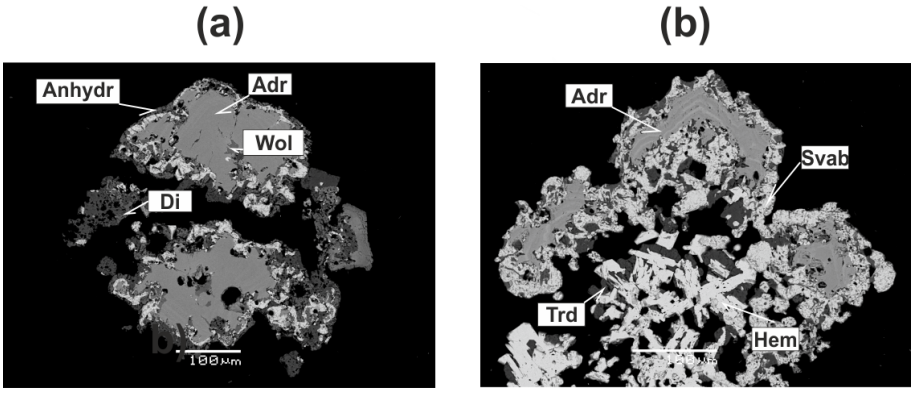

Figure 4. Zonal crystals and crusts of andradite (Adr) in association with diopside (Di), anhydrite (Anhydr), svabite (Svab), hematite (Hem), wollastonite (Wol) and tridymite (Trd). BSE images.

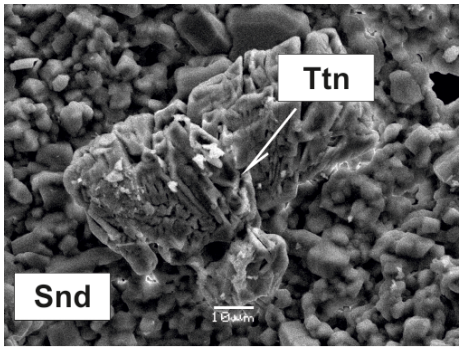

Figure 5. Split titanite crystals overgrowing sanidine crust. SE image.

sisting of well-shaped short-prismatic crystals (up to 0.2 mm in size) and open-work aggregates overgrowing basalt scoria or hematite crusts (Fig. 8b). The colour of diopside is variable: bright yellow, orange, brownish green, green, light brown or reddish brown, to brown red or brick red. Aegirine in the Arsenatnaya fumarole occurs as elongated light yellow to bright sulfur-yellow prismatic crystals up to 0.3 mm (Fig. 7c, d) associated with hematite, fluorophlogopite, sanidine, sodalite, cassiterite, Na-rich sylvite and various arsenates. Esseneite forms tiny (10–20 µm in size) inclusions in anorthoclase and sanidine or areas in diopside crystals in Zones IVa and IVb.

The chemical composition of these clinopyroxenes varies widely. The $Al:Fe^{3+}$ and $Ca:Na$ ratios in members of the discussed solid–solution system are shown in Fig. 9. Diopside is characterized by both $Mg:Fe^{3+}$ ratio and content of Al_2O_3 varying significantly (from 0.00 to 0.49 Al apfu). It forms a solid solution with esseneite, ideally $CaFe^{3+}[AlSiO_6]$, with a distinct positive correlation between Al^{3+} and Fe^{3+} contents. The absence of the hedenbergite component $CaFe^{2+}[Si_2O_6]$ is due to the highly oxidizing conditions of mineral formation. The $Si:Al$ ratio in pyroxenes of the diopside–esseneite–aegirine system varies as displayed in Fig. 9c. The linear dependence demonstrates that Al preferably occupies the tetrahedral sites in the structure. The deviation to the left from the ideal line is connected with As^{5+} or Fe^{3+} impurities and to the right with abundance of Al for tetrahedral sites.

The single-crystal structure refinement of a $Na-Al-Fe^{3+}$-rich variety of diopside ($a = 9.7468(15)$, $b = 8.8797(14)$, $c = 5.2819(8)$ Å, $\beta = 105.906(2)°$, $V = 439.64(12)$ Å^3; space group $C2/c$; on the basis of 677 independent reflections with $I > 2\sigma(I) F > 2\sigma$ to $R_1 = 2.89$ %) confirms that Fe^{3+} preferably occupies the octahedral site while Al prefers the tetrahedral site. The octahedral site $M(2)$ was refined as being occupied by Mg and Fe^{3+} ($e_{ref} = 15.4$); the content of Al at T site was derived from the chemical composition of studied crystal, because Si and Al are not distinguishable by routine XRD analysis due to similar scattering amplitudes. The crystal-chemical formula is $(Ca_{0.85}Na_{0.15})_{\sum 1.00}(Mg_{0.76}Fe^{3+}_{0.24})_{\sum 1.00}[(Si_{1.85}Al_{0.15})_2O_6]$.

Another solid–solution series is found between diopside and aegirine, including aegirine-augite with 0.30–0.43 Na apfu (Fig. 9b).

Diopside from the Arsenatnaya fumarole contains (up to, wt %) 1.2 CuO, 0.3 ZnO, 7.0 SnO_2 and 2.6 As_2O_5. The main chalcophile components in aegirine are As_2O_5 (up to 0.8 wt %) and SnO_2 (up to 0.3 wt %). In esseneite up to 2.1 wt % As_2O_5 was detected.

5.2.3 Cu,Mg-pyroxene

In addition to these pyroxenes common for the Arsenatnaya fumarole, a specific Cu-rich pyroxene was found in several samples (Table 3, analyses 17–19). Its average empirical formula is $Mg_{1.00}(Cu_{0.76}Mg_{0.15}Zn_{0.08}Fe^{3+}_{0.03})_{\sum 1.01}$ $[Si_{1.93}Al_{0.05}Fe^{3+}_{0.02})_{\sum 2.00}O_6]$. This pyroxene forms thin greenish-brown or brown crust (up to 7 µm thick) on crystals of light brown diopside (Fig. 8c). The insufficient quality of the powder XRD pattern of this Cu-rich pyroxene (due

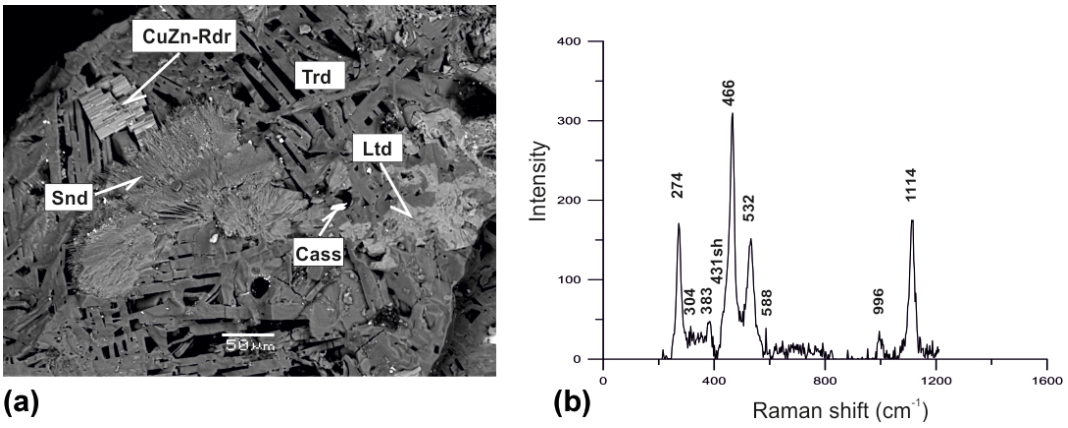

Figure 6. Parallel intergrowth of prismatic crystals of a Cu,Zn-rich analogue of roedderite (CuZn-Rdr) on aggregate of platy crystals of tridymite (Trd) in association with sanidine (Snd), litidionite (Ltd) and cassiterite (Cass). BSE image **(a)**; Raman spectrum of randomly oriented sample of Cu,Zn-rich analogue of roedderite from the Arsenatnaya fumarole **(b)**.

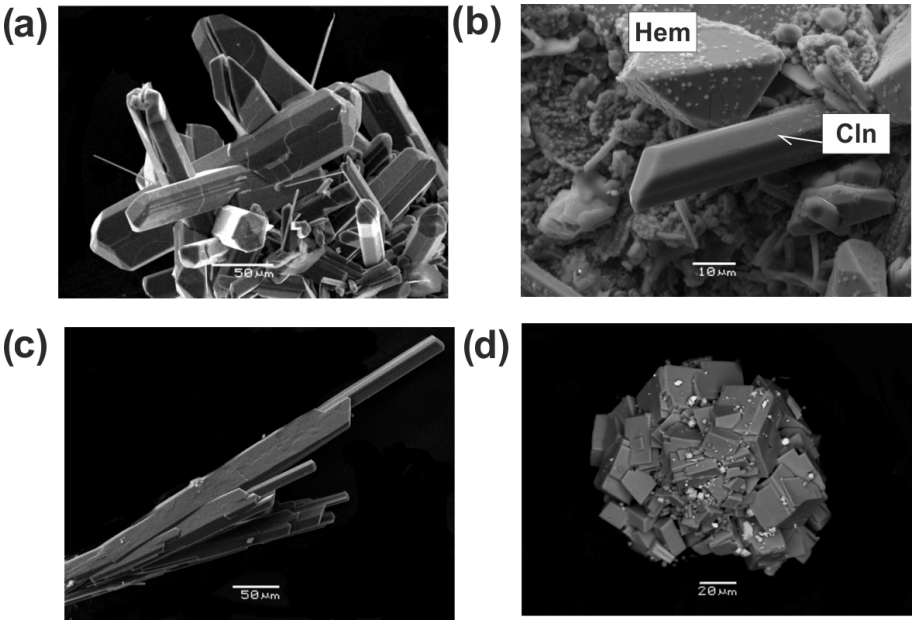

Figure 7. Pyroxenes from the Arsenatnaya fumarole: **(a)** aggregate of prismatic crystals of enstatite; **(b)** well-shaped prismatic crystals of clinoenstatite (Cln) in association with hematite (Hem); **(c)** sheaf-like cluster of long-prismatic crystals of aegirine (Aeg); **(d)** cluster of short-prismatic crystals of aegirine. SEM images: **(a, c, b)** SE images; **(d)** BSE image.

to scarcity of pure material) hampers the determination of its crystallographic characteristics. By analogy with data on the synthetic pyroxene $CuMg[Si_2O_6]$ possessing the enstatite-type structure (Tachi et al., 1997), we suggest that this mineral could be orthorhombic. Unit-cell dimensions calculated from powder XRD data based on this assumption are given in Table 1.

5.2.4 Wollastonite

A mineral with the Ca : Si ratio very close to 1 : 1 was detected in the core of one andradite crystal (Fig. 4a). The small size of this inclusion (about 10 μm) made it impossible to determine the polymorph of $CaSiO_3$. However, the conditions of mineral formation in the Arsenatnaya fumarole allow us to suggest that this silicate is probably common wollastonite, which is stable in the pressure range 0–30 kbar and at temperatures less than 1130 °C (Swamy and Dubrovinsky, 1997). This mineral from the Arsenatnaya fumarole contains (wt %): 0.7 Fe_2O_3, 0.2 MgO, 0.3 MnO and 0.4 As_2O_5 (Table 3, analysis 20).

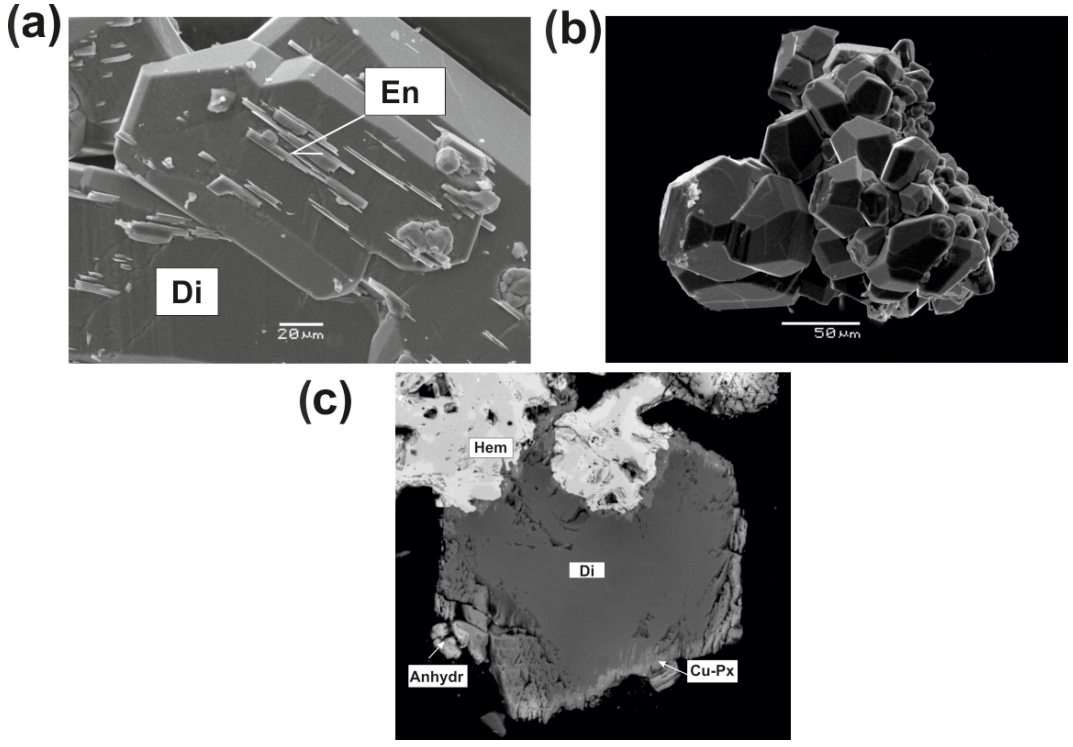

Figure 8. Pyroxenes from the Arsenatnaya fumarole: **(a)** diopside (Di) crystal overgrown by enstatite (En) crystals; **(b)** aggregates of well-shaped crystals of diopside; **(c)** crystal of diopside (Di) covered by thin crust of Cu,Mg-pyroxene (Cu-Px) in association with anhydrite (Anhydr) and hematite (Hem) (FOV width is 0.25 mm). **(a, c)** BSE images; **(b)** SE image.

5.2.5 Potassic-fluoro-magnesio-arfvedsonite and potassic-fluoro-richterite

Amphiboles in the Arsenatnaya fumarole are represented by potassic-fluoro-magnesio-arfvedsonite, ideally $KNa_2(Mg_4Fe^{3+})[Si_8O_{22}]F_2$, and potassic-fluoro-richterite, ideally $KNaCaMg_5[Si_8O_{22}]F_2$, which occur in the arsenate-enriched Zone IV. These amphiboles form tiny split acicular white, colourless, yellow or dark-green crystals and their shaggy aggregates (Fig. 10a, b, d).

Amphiboles from Arsenatnaya contain up to 3.6 wt % As_2O_5. The representative empirical formulae of the studied potassic-fluoro-magnesio-arfvedsonite and potassic-fluoro-richterite are $(K_{0.98}Na_{0.02})_{\sum 1.00}Na_{2.01}(Mg_{3.93}Fe^{3+}_{0.52}Ca_{0.29}Cu_{0.19}Mn_{0.02}Ti_{0.02})_{\sum 4.97}[(Si_{7.65}As_{0.18}Zn_{0.08}Fe^{3+}_{0.05}V^{5+}_{0.03}Al_{0.01})_{\sum 8.00}O_{22}]F_{1.86}Cl_{0.06}$ and $K_{0.66}(Na_{1.21}Ca_{0.80})_{\sum 2.01}(Mg_{4.10}Fe^{3+}_{0.69}Ca_{0.10}Ti_{0.07}Sn_{0.03})_{\sum 4.99}[(Si_{7.58}Al_{0.32}Fe^{3+}_{0.10})_{\sum 8.00}O_{22}]F_{1.66}O_{0.13}$ respectively.

5.2.6 Litidionite

Litidionite occurs as bright blue coarse prismatic crystals up to 0.02 mm long growing on sylvite, as balls up to 60 μm in diameter on aggregates of Na-bearing sylvite and as lamellar aggregates overgrowing tridymite (Fig. 10c, d). Its chemical composition is very close to the end-member $KNaCu[Si_4O_{10}]$ (Table 3, analysis 23). The empirical formula of its typical sample is $K_{0.97}Na_{1.06}Cu_{1.00}Zn_{0.02}Fe^{3+}_{0.01}V^{5+}_{0.01}Si_{3.97}O_{10}$.

5.3 Phyllosilicates

5.3.1 Fluorophlogopite

Fluorophlogopite, ideally $KMg_3[AlSi_3O_{10}]F_2$, is one of the major silicates in the Arsenatnaya fumarole. This mica forms monomineralic crusts up to several hundred square centimetres in area which overgrow or replace basalt scoria in Zones Va, Vb and VIa. It is associated with sanidine, arsenates of the alluaudite group, anhydrite, hematite, sylvite, halite, aphthitalite-group sulfates, etc. Fluorophlogopite occurs as brushes, open-work aggregates and clusters consisting of pseudo-hexagonal flattened crystals up to 0.5 mm across in cracks and cavities (Fig. 11). The colour of the mineral varies from vivid orange and light brown to pale yellow or white; thin flakes are colourless.

The main difference between this fluorophlogopite and typical phlogopite–fluorophlogopite series from other geological formations is the absence of hydroxyl groups in samples from Arsenatnaya (Table 3, analyses 24 and 25). This is confirmed by both IR and Raman spectroscopy data. The

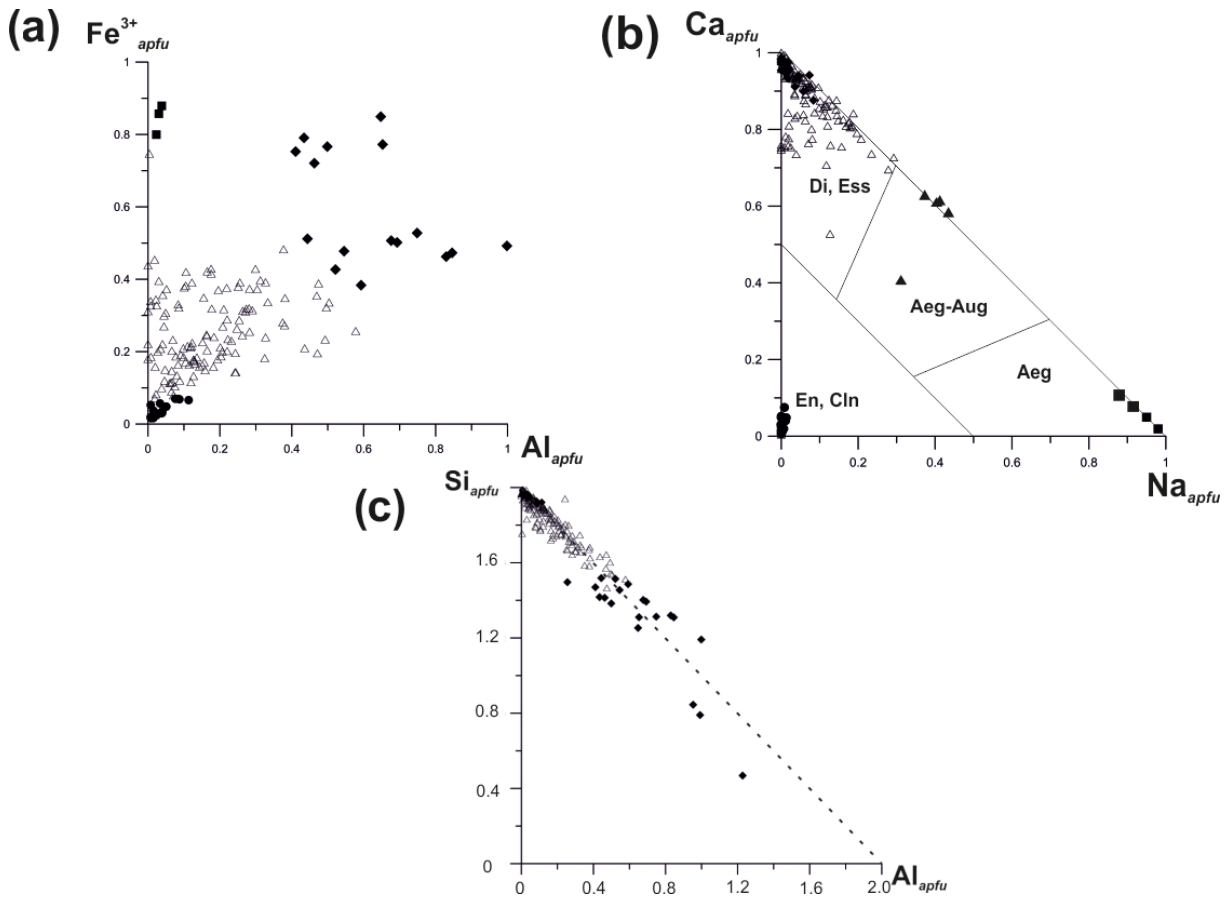

Figure 9. Ratios of Fe^{3+} to Al (total, i.e. octahedrally and tetrahedrally coordinated Al) **(a)**, Ca to Na **(b)** and Si to Al (total, i.e. both octahedrally and tetrahedrally coordinated Al) **(c)** in pyroxenes of the diopside (Di)–aegirine (Aeg)–esseneite (Ess) solid–solution system from the Arsenatnaya fumarole: ■ – aegirine, ▲ – aegirine-augite, ● – enstatite and clinoenstatite, ♦ – esseneite, △ – diopside. The type of diagram **(b)** was proposed by Morimoto et al. (1988).

content of O_2 substituting F^- in the mineral from Arsenatnaya reaches 0.30 apfu.

The main characteristic impurities in fluorophlogopite from the Arsenatnaya fumarole are (up to, wt %) 5.1 As_2O_5, 1.0 CuO, 1.7 ZnO, 0.8 SnO_2 and 0.9 P_2O_5. The mineral contains not more than 4.1 wt % Fe_2O_3 (0.22 Fe^{3+} apfu).

Fluorophlogopite from the Arsenatnaya fumarole is represented by the ordinary monoclinic 1*M* polytype (Table 1).

5.3.2 Fluoreastonite

Another mica with the idealized formula $K(Mg, Al)_3[Al_2Si_2O_{10}](F, O)_2$ (Table 3, analysis 26) was found in the same associations. It forms thin flakes closely intergrown with fluorophlogopite. This mica is considered fluoreastonite, a F-dominant analogue of eastonite, ideally $KMg_2Al[Al_2Si_2O_{10}](OH)_2$.

5.3.3 Yangzhumingite

This mica, visually identical to fluorophlogopite, corresponds to the idealized formula $KMg_{2.5}[Si_4O_{10}]F_2$. It was considered to be yangzhumingite (Miyawaki et al., 2011) and identified only in a few samples.

Yangzhumingite contains impurities of As_2O_5 (up to 0.6 wt %) and CuO (up to 1.4 wt %) (Table 3, analyses 27 and 28). Its representative empirical formulae are $(K_{0.86}Na_{0.17})_{\sum 1.03}(Mg_{2.49}Cu_{0.08}Ti_{0.02})_{\sum 2.59}[(Si_{3.76}Fe^{3+}_{0.11}Al_{0.09}Zn_{0.04}As_{0.02})_{\sum 4.02}O_{10}]F_{1.93}$ and $(K_{0.72}Na_{0.03})_{\sum 0.75}(Mg_{2.74}Cu_{0.02}Mn_{0.01})_{\sum 2.77}[(Si_{3.76}Al_{0.19}Fe^{3+}_{0.04})_{\sum 3.99}O_{10}]F_{1.97}$.

5.3.4 Sn analogue of dalyite

A mineral with chemical composition very close to the formula $K_2Sn[Si_6O_{15}]$ occurs as tabular patches up to 0.05 mm across (Fig. 12), in association with tin-bearing varieties of arsmirandite (up to 1 wt % SnO_2) and potassic-fluoromagnesio-arfvedsonite (up to 1.2 wt % SnO_2) and with cassi-

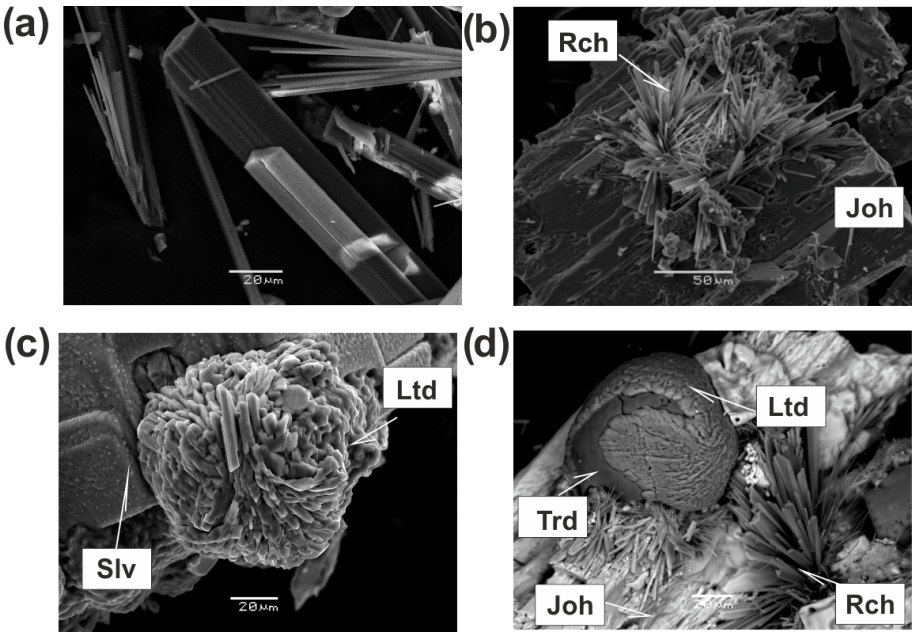

Figure 10. Long-prismatic to acicular crystals of potassic-fluoro-magnesio-arfvedsonite **(a)**, bush-like clusters of acicular crystals of potassic-fluoro-richterite (Rch) overgrowing johillerite (Joh) **(b)**, spherulite of litidionite consisting of split crystals on sylvite (Slv) **(c)** and shaggy aggregates of potassic-fluoro-richterite (Rch), with tridymite (Trd) spherulite partially covered by litidionite (Ltd) on crystal of johillerite (Joh) **(d)**. **(a–c)** SE images; **(d)** BSE image.

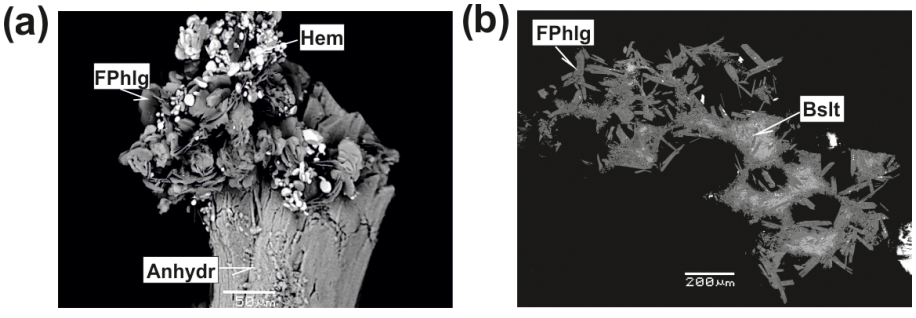

Figure 11. Fluorophlogopite (FPhlg) from the Arsenatnaya fumarole: **(a)** clusters powdered by hematite (Hem) on anhydrite (Anhydr); **(b)** aggregates replacing basalt scoria (Bslt). BSE images.

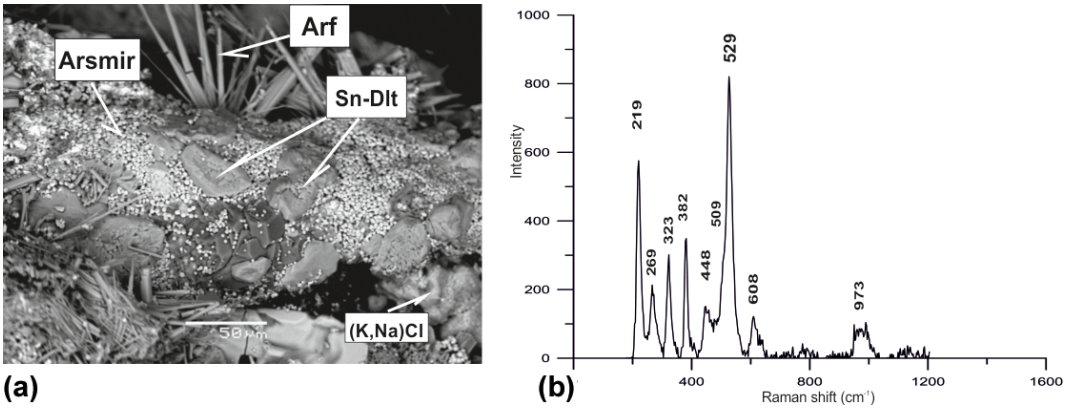

Figure 12. Patch-like crystals of the Sn analogue of dalyite (Sn-Dlt) on arsmirandite (Arsmir) in association with potassic-fluoro-magnesio-arfvedsonite (Arf) and Na-bearing sylvite [(K,Na)Cl]; BSE image **(a)**. Raman spectrum of randomly oriented sample of Sn analogue of dalyite from the Arsenatnaya fumarole **(b)**.

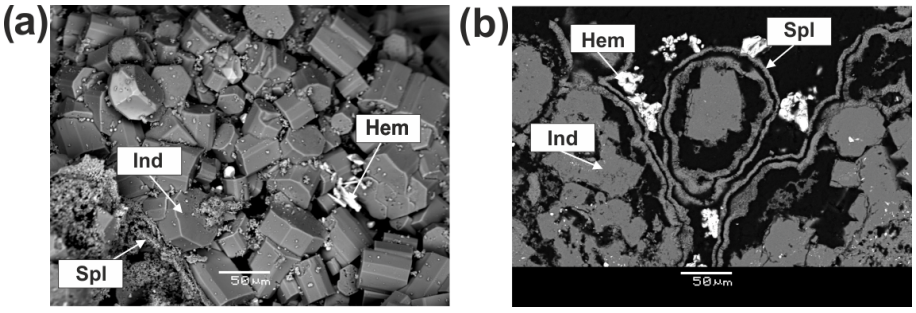

Figure 13. Crystals of indialite (Ind) overgrown by spinel (Spl) in association with hematite (Hem). Mountain 1004. BSE images.

terite. Both stoichiometry and the Raman spectrum (Fig. 12) demonstrate that this mineral is the Sn analogue of dalyite, $K_2Zr[Si_6O_{15}]$, and davanite, $K_2Ti[Si_6O_{15}]$. Noteworthy is that there are also intermediate members of the $K_2Ti[Si_6O_{15}]$–$K_2Sn[Si_6O_{15}]$ series (Table 3, analysis 30).

6 Silicate mineralization of the ancient fumarolic fields of Mountain 1004

In southern and western paleofumarolic fields of Mountain 1004 we have identified enstatite, diopside, fluorophlogopite, sanidine, anorthoclase, leucite, hauyne and indialite. These silicates overgrow or replace basalt scoria altered by fumarolic gas. They are closely associated with hematite and sometimes with tenorite, spinel-group oxides (including Cu-bearing varieties of gahnite and magnesioferrite; Pekov et al., 2018b), corundum, fluorite, sellaite, anglesite, baryte, fluorapatite–pliniusite series minerals, svabite, johillerite and kainotropite.

The chemical composition of cyclo-, ino- and phyllosilicates from paleofumaroles of Mountain 1004 is given in Table S2. In contrast to data reported by Naboko and Glavatskykh (1992), enstatite and fluorophlogopite studied by the authors contain admixed copper (up to 0.3 and 5.9 wt % CuO respectively). All studied samples of mica are fluorophlogopite with a F content close to 2.0 apfu.

Indialite deserves special attention. Unlike other abovementioned silicates, it was found at Tolbachik only within the western paleofumarole field of Mountain 1004. This high-temperature hexagonal dimorph of cordierite was identified using powder XRD. The characteristic reflections of the powder XRD pattern of indialite from the Mountain 1004 are (d in ångströms, I) 8.47 (100), 4.89 (22), 4.09 (35), 3.38 (37), 3.14 (44), 3.03 (40), 2.64 (13) and 1.69 (14). The main characteristic of the XRD pattern of cordierite dimorphous with indialite is the presence of three well-resolved peaks in the range $d = 3.05$–3.01 Å, whereas indialite shows a single reflection at $d \approx 3.03$ Å (Miyashiro, 1957). The presence of this single peak in the X-ray diffraction pattern allows us to identify the mineral from Mountain 1004 as indialite. It occurs as well-shaped short prismatic hexagonal crystals up to 50 μm in size associated with corundum and spinel (Fig. 13). The representative empirical formula of indialite from Mountain 1004 is $Ca_{0.01}Mg_{2.00}[(Si_{4.73}Al_{4.32}Fe^{3+}_{0.04})_{\sum 9.09}]O_{18}$.

Data availability. All data used are given in the tables, figures and text and in the Supplement to this paper.

Supplement. The supplement related to this article is available online at: https://doi.org/10.5194/ejm-32-101-2020-supplement.

Author contributions. NVS and IVP wrote the paper. NVS and NVZ carried out the crystal structure analysis. NVS obtained Raman spectroscopic data. NVS and SNB obtained and processed the X-ray diffraction data. NNK and DAV processed electron microprobe. IVP and EGS collected and prepared samples.

Competing interests. The authors declare that they have no conflict of interest.

Acknowledgements. We thank the two anonymous reviewers for their valuable comments and Sergey V. Krivovichev and Christian Chopin for the editing work. This work was supported by the Russian Science Foundation, grant no. 19-17-00050 (as part of mineralogical studies), and the Russian Foundation for Basic Research, grant 18-05-00332 (as part of XRD and structural studies of pyroxenes). The technical support by the SPbSU X-Ray Diffraction Resource Center is acknowledged.

Review statement. This paper was edited by Sergey Krivovichev.

References

Agilent Technologies: CrysAlisPro Software system, version 1.171.37.35. Agilent Technologies UK Ltd., Oxford, UK, 2014.

Africano, F. and Bernard, A.: Acid alteration in the fumarolic environment of Usu volcano, Hokkaido, Japan, J. Volcan. Geoth. Res., 97, 475–495, 2000.

Alietti, E., Brigatti, M. F., Capedri, S., and Poppi, L.: The roedderite-chayesite series from Spanish lamproites: Crystal-chemical characterization, Mineral. Mag., 58, 655–662, 1994.

Balić-Žunić, T., Garavelli, A., Jakobsson, S. P., Jonasson, K., Katerinopoulos, A., Kyriakopoulos, K., and Acquafredda, P.: Fumarolic minerals: an overview of active European volcanoes, in: Updates in Volcanology – From Volcano Modelling to Volcano Geology, edited by: Nemeth, K., 267–322, InTech Open Access Publishers, 2016.

Britvin, S. N., Dolivo-Dobrovolsky, D. V., and Krzhizhanovskaya, M. G.: Software for processing the X-ray powder diffraction data obtained from the curved image plate detector of Rigaku RAXIS Rapid II diffractometer, Zapiski RMO, 146, 104–107, 2017 (in Russian).

Campostrini, I., Demartin, F., Gramaccioli, C. M., and Russo, M.: Vulcano: Tre Secoli di Mineralogia, Associazione Micromineralogica Italiana, Cremona, 2011.

Chaplygin, I. V., Mozgova, N. N., Mokhov, A. V., Koporulina, E. V., Bernhardt, H. J., and Bryzgalov, I. A.: Minerals of the system ZnS-CdS from fumaroles of the Kudriavy volcano, Iturup Island, Kuriles, Russia, Can. Mineral., 45, 709–722, 2007.

Fedotov, S. A. and Markhinin, Y. K. (Eds.): The Great Tolbachik Fissure Eruption, Cambridge University Press, New York, 1983.

Getahun, A., Reed, M. H., and Symonds, R.: Mount St. Augustine volcano fumarole wall rock alteration: mineralogy, zoning, composition and numerical models of its formation process, J. Volcan. Geoth. Res., 71, 73–107, 1996.

Hawthorne, F. C., Oberti, R., Harlow, G. E., Maresch, W. V., Martin, R. F., Schumacher, J. C., and Welch, M. D.: Nomenclature of the amphibole supergroup, Am. Mineral., 97, 2031–2048, 2012.

Honnorez, J., Honnorez-Guerstein, B., Valette, J., and Wauschkuhn, A.: Present day formation of an exhalative sulfide deposit at Vulcano (Thyrrhenian Sea), Part II: active crystallization of fumarolic sulfides in the volcanic sediments of the Baia di Levante, Ores Sedim., 3, 139–166, 1973.

Keith, T. E., Casadevall, T. J., and Johnston, D. A.: Fumarole encrustations: occurrence, mineralogy, and chemistry, Geol. Surv. Prof. Paper, 239–250, 1981.

Morimoto, N., Fabries, J., Ferguson, A. K., Ginzburg, I. V., Ross, M., Seifert, F. A., and Zussman, J.: Nomenclature of pyroxenes, Mineral. Mag., 52, 535–550, 1988.

Miyashiro, A.: Cordierite-indialite relations, Am. J. Sci., 255, 43–62, 1957.

Miyawaki, R., Shimazaki, H., Shigeoka, M., Yokoyama, K., Matsubara, S., and Yurimoto, H.: Yangzhumingite, $KMg_{2.5}Si_4O_{10}F_2$, a new mineral in the mica group from Bayan Obo, Inner Mongolia, China. Eur. J. Mineral., 23, 467–473, 2011.

Naboko, S. I. and Glavatskikh, S. F.: Relics of posteruptive activity on old cones of the Tolbachik Dale, Kamchatka, Vulkan. Seism., 5–6, 66–86, 1992. (in Russian).

Naughton, J. J., Greenberg, V. A., and Goguel, R.: Incrustations and fumarolic condensates at Kilauea volcano, Hawaii: field, drill-hole and laboratory observations, J. Volcan. Geoth. Res., 1, 149–165, 1976.

Pekov, I. V., Zubkova, N. V., Yapaskurt, V. O., Belakovskiy, D. I., Lykova, I. S., Vigasina, M. F., Sidorov, E. G., and Pushcharovsky, D. Yu.: New arsenate minerals from the Arsenatnaya fumarole, Tolbachik volcano, Kamchatka, Russia – I. Yurmarinite, $Na_7(Fe^{3+}, Mg, Cu)_4(AsO_4)_6$, Mineral. Mag., 78, 905–917, 2014.

Pekov, I. V., Koshlyakova, N. N., Zubkova, N. V., Lykova, I. S., Britvin, S. N., Yapaskurt, V. O., Agakhanov, A. A., Shchipalkina, N. V., Turchkova, A. G., and Sidorov, E. G.: Fumarolic arsenates – a special type of arsenic mineralization, Eur. J. Mineral., 30, 305–322, 2018a.

Pekov, I. V., Sandalov, F. D., Koshlyakova, N. N., Vigasina, M. F., Polekhovsky, Y. S., Britvin, S. N., Sidorov, E. G., and Turchkova, A. G.: Copper in natural oxide spinels: the new mineral thermaerogenite $CuAl_2O_4$, cuprospinel and Cu-enriched varieties of other spinel-group members from fumaroles of the Tolbachik volcano, Kamchatka, Russia, Minerals, 8, paper no. 498, 2018b.

Pekov, I. V., Agakhanov, A. A., Zubkova, N. V., Koshlyakova, N. N., Shchipalkina, N. V., Sandalov, F. D., Yapaskurt, V. O., Turchkova, A. G., and Sidorov, E. G.: Oxidizing-type fumarolic systems of the Tolbachik volcano – a mineralogical and geochemical unique, Russ. Geol. Geophys., https://doi.org/10.15372/GiG2019167, in press, 2020.

Petriček, V., Dušek, M., and Palatinus, L.: Crystallographic Computing System JANA2006: General features, Z. Kristallogr., 229, 345–352, 2014.

Serafimova, E. K.: Mineralogy of Sublimates at Kamchatka Volcanoes, Nauka Publishing, Moscow, 1979 (in Russian).

Serafimova, E. K.: Mineral paragenesis of volcanic exhalations. Post-eruptive mineral formation on active volcanoes of Kamchatka, PI, Far Eastern Branch of RAS, 31–52, 1992 (in Russian).

Serafimova, E. K., Semenova, T. F., and Sulimova, N. V.: The copper and lead minerals from ancient fumarole fields of Mountain 1004 (Kamchatka), Vulkan. Seism., 3, 35–49, 1994 (in Russian).

Sharygin, V. V, Kamenetsky, V. S., Zhitova, L. M., Belousov, A. B., and Abersteiner, A.: Copper-containing magnesioferrite in vesicular trachyandesite in a lava tube from the 2012–2013 eruption of the Tolbachik volcano, Kamchatka, Russia, Minerals, 8, paper no. 514, 2018.

Shchipalkina, N. V., Pekov, I. V., Zubkova, N. V., Koshlykova, N. N., and Sidorov, E. G.: Natural forsterite strongly enriched by arsenic and phosphorus: chemistry, crystal structure, crystal morphology and zonation, Phys. Chem. Minerals, 46, 889–898, 2019.

Shchipalkina, N. V., Pekov, I. V., Koshlyakova, N. N., Britvin, S. N., Zubkova, N. V., Varlamov, D. A., and Sidorov, E. G.: Unusual silicate mineralization in fumarolic sublimates of the Tolbachik volcano, Kamchatka, Russia – Part 2: Tectosilicates, Eur. J. Mineral., 32, 121–136, https://doi.org/10.5194/ejm-32-121-2020, 2020.

Smyth, J. R.: Experimental study on the polymorphism of enstatite, Am. Mineral., 59, 345–352, 1974.

Stoiber, R. E. and Rose, W. I.: Fumarole incrustation at active Central American volcanoes, Geochim. Cosmochim. Ac., 38, 495–516, 1974.

Swamy, V. and Dubrovinsky, L. S.: Thermodynamic data for the phases in the $CaSiO_3$ system, Geochim. Cosmochim. Ac., 61, 1181–1191, 1997.

Symonds, R. B., Rose, W. I., Reed, M. H., Lichte, F. E., and Finnegan, D. L.: Volatilization, transport and sublimation of metallic and non-metallic elements in high temperature gases

at Merapi Volcano, Indonesia, Geochem. Cosmochim. Ac., 51, 2083–2101, 1987.

Tachi, T., Horiuchi, H., and Nagasawa, H.: Structure of Cu-bearing orthopyroxene, $Mg(Cu_{0.56}Mg_{0.44})Si_2O_6$, and behavior of Cu^{2+} in the orthopyroxene structure, Phys. Chem. Minerals, 24, 463–476, 1997.

Tessalina, S. G., Yudovskaya, M. A., Chaplygin, I. V., Birck, J. L., and Capmas, F.: Sources of unique rhenium enrichment in fumaroles and sulphides at Kudryavy volcano, Geochim. Cosmochim. Ac., 72, 889–909, 2008.

Vergasova, L. P. and Filatov, S. K.: A study of volcanogenic exhalation mineralization, J. Volcanol. Seismol., 10, 71–85, 2016.